Auger decay of $1\sigma_g$ and $1\sigma_u$ hole states of the N_2 molecule. II. Young-type interference of Auger electrons and its dependence on internuclear distance

N. A. Cherepkov,[1,2] S. K. Semenov,[1] M. S. Schöffler,[2] J. Titze,[2] N. Petridis,[2] T. Jahnke,[2] K. Cole,[2] L. Ph. H. Schmidt,[2] A. Czasch,[2] D. Akoury,[2,3] O. Jagutzki,[2] J. B. Williams,[4] T. Osipov,[3] S. Lee,[3] M. H. Prior,[3] A. Belkacem,[3] A. L. Landers,[4] H. Schmidt-Böcking,[2] R. Dörner,[2] and Th. Weber[3]

[1]*State University of Aerospace Instrumentation, 190000 St. Petersburg, Russia*

[2]*Institut für Kernphysik, University Frankfurt, Max-von-Laue-Strasse 1, D-60438 Frankfurt, Germany*

[3]*Lawrence Berkeley National Labararatory, Berkeley, California 94720, USA*

[4]*Department of Physics, Auburn University, Auburn, Alabama 36849, USA*

(Received 18 June 2010; published 25 August 2010)

Theoretical two-center interference patterns produced (i) by the *K*-shell photoionization process of the N_2 molecule and (ii) by the Auger decay process of the *K*-shell hole state of the N_2 molecule are compared for the case of equal photo- and Auger-electron energies of about 360 eV. The comparison shows that both the angular distribution of the photoelectrons and the angular distribution of the Auger electrons of equal energy in the molecular frame are primarily defined by the Young interference. The experimental data for the angular resolved *K*-shell Auger electrons as a function of the kinetic-energy release (KER) obtained earlier [Phys. Rev. A **81**, 043426 (2010)] have been renormalized in order to visualize the angular variation in the regions of low Auger-electron intensities. That renormalized data are compared with the corresponding theoretical results. From the known behavior of the potential energy curves, the connection between the KER and the internuclear distance can be established. Since the Young interference pattern is sensitive to the internuclear distance in the molecule, from the measured KER dependence of the Young interference pattern one can trace the behavior of the Auger-electron angular distribution for different molecular terms as a function of internuclear distance. The results of that analysis are in a good agreement with the corresponding theoretical predictions.

DOI: 10.1103/PhysRevA.82.023420 PACS number(s): 33.80.Eh

I. INTRODUCTION

The famous Young's double-slit experiment demonstrated how the addition of two coherent waves of light leads to interference oscillations of the light intensity as a function of direction of light propagation. A conceptually similar phenomenon for the photoelectron waves emitted from homonuclear diatomic molecules has been discussed in a number of papers [1–4]. Instead of passing through the holes in a screen, the photoelectron is ejected from a state described as a linear combination of two atomic orbitals localized on different atoms. The interference of the coherent electron waves emitted from two indistinguishable atoms leads to intrinsic interference oscillations. To observe this pattern one must study photoemission from fixed-in-space molecules. Recently, this molecular double-slit pattern was observed in a more complicated case of double photoionization of the H_2 molecule, where the dissociation of the two protons allows the molecule to be fixed in space by coincidence detection of electrons and protons. If one of the electrons is very slow while the other one takes nearly all excess energy, the angular distribution of the fast electron clearly exhibits the interference pattern [5–9].

Cohen and Fano [10] have shown that even the total photoionization cross section for the H_2 molecule oscillates as a function of photon energy due to the presence of the Young's interference. Recently these oscillations have been studied both theoretically and experimentally for the H_2 [11] and N_2 [12,13] molecules. These oscillations are also seen in the electron spectra from charged- particle impact ionization of molecules [14,15]. In the case of the N_2 molecule it was necessary to resolve the contributions of the $1\sigma_g$ and $1\sigma_u$ core levels, which are separated by a very small energy gap of about 0.1 eV. That became possible only recently owing to the application of the modern high-resolution x-ray photoelectron spectroscopy using synchrotron radiation as a light source [16,17]. Results of the experiments [12,13] clearly exhibited the Cohen-Fano interference modulation of the partial photoionization cross sections for the $1\sigma_g$ and $1\sigma_u$ shells (which are in antiphase), in a good agreement with the predictions of the theory developed there.

Applications of different coincidence techniques during the last 15 years made it possible to study the angular distributions of photoelectrons from fixed-in-space molecules in the gas phase (see [18–25] and references therein). However, up to now, to our knowledge, there have been no direct studies of the Young's interference pattern for photoelectron waves emitted from fixed-in-space N_2 molecules at the relatively high photon energies (770 eV) considered in this paper.

Auger electrons resulting from the decay of core levels in homonuclear diatomic molecules like N_2 can also exhibit the Young's interference pattern provided the decay processes of the $1\sigma_g$ and $1\sigma_u$ states are separated. As far as we know, that has also not been studied up to now. In this paper we compare the molecular frame theoretical angular distributions of photoelectrons and Auger electrons of equal energies resulting from the $1\sigma_g$ and $1\sigma_u$ core levels of a N_2 molecule and demonstrate that they are essentially defined by the Young's interference pattern. Since this pattern depends on the distance between the slits, or on the internuclear distance in the case of the N_2 molecule, the study of the Young's interference pattern must allow, in particular, a determination of the internuclear distance at the moment of the Auger decay. Experimental studies capable of discovering such a phenomenon have been performed very recently and are presented in our previous publications [26,27].

A careful analysis of those experimental data enabled us to disentangle the dependence of the Young's interference pattern on the internuclear distance, which appears to be in a good agreement with our calculations. The present paper is a direct continuation of the study presented in [26,27], where a detailed description of both theory and experiment was given, and we do not repeat it here. Reference [27] will be referred to further as I.

Photoionization of the K shell of a N_2 molecule produces a highly excited molecular ion state which decays within a short time of about 7 fs, predominantly by emission of a fast Auger electron (around 360 eV). In a two-step model which is implied to be valid in our case the Auger decay does not depend on the energy of the photon which produced the K-hole state (the photon energy in our experiment was equal to 419 eV). As a result, a doubly charged molecular ion is created with two holes in the valence shell(s). At the next step this doubly charged molecular ion dissociates predominantly into two N^+ atomic ions with kinetic energy release (KER) in the region of 4–20 eV. The dissociation time is usually short compared to the molecular rotation; therefore the direction of motion of the atomic ions gives the direction of the molecular axis at the time of both photoabsorption and Auger decay.

In our experiment the Auger-decay process was studied by detecting in coincidence the photoelectron and the two atomic singly charged ions (all of them being energy and angular resolved) using the cold target recoil ion momentum spectroscopy technique [21,23,25–29]. The Auger-electron ejection angle was determined from the known momenta of three other particles using the momentum conservation law. From calculations it is known that at some angles of photoelectron emission the $1\sigma_g$ or $1\sigma_u$ shell is the primary contributor [25–27]. By determination of the Auger-electron angular distribution in coincidence with the photoelectrons collected at these angles, the contributions of the $1\sigma_g$ and $1\sigma_u$ shells to the Auger-decay process were separated without resolving these transitions in energy.

II. PHOTOELECTRON ANGULAR DISTRIBUTIONS

The electron densities of the $1\sigma_g$ and $1\sigma_u$ orbitals of the N_2 molecule are confined near individual nuclei, and a photoelectron is emitted from either of the two centers with equal probabilities. As a result, Young interference of the two electron waves originating from two centers must appear. Let R be the internuclear distance ($R = 2.068$ a.u. at equilibrium in the the ground state of N_2) and η be the angle between the direction of observation and the direction perpendicular to the molecular axis. For a photoelectron of energy $E = 360$ eV (which is equal to the Auger-electron energy considered below), the wavelength λ is equal to 1.22 a.u. and is of the same order of magnitude as the internuclear distance R. That is the main precondition for the appearance of the Young interference pattern. The corresponding photoelectron momentum is $k = 2\pi/\lambda = 5.14$ a.u. The wave function of the $1\sigma_g$ shell has the same sign on both centers; therefore the photoelectron waves emitted from the two centers have equal phases. As a result, in the direction perpendicular to the molecular axis the interference maximum appears. The first interference minima are placed at the angles defined by the equation $\sin\eta = \lambda/2R = \pi/kR$, which in our case correspond to $\eta = \pm 17^\circ$. Analogously, the first-order maxima appear at the angles defined by the equation $\sin\eta = \lambda/R$, which gives $\eta = \pm 36^\circ$.

The wave function of the $1\sigma_u$ shell has opposite signs on the two centers, and so the corresponding photoelectron waves differ in phase by π. Therefore in the direction perpendicular to the molecular axis there is the interference minimum; the first-order maxima appear at the angles defined by the equation $R\sin\eta = \lambda/2$, that is, at $\eta = \pm 17^\circ$, and correspondingly the first-order minima appear at the angles $\eta = \pm 36^\circ$. In other words, the interference oscillations of the photoelectron waves emitted from the $1\sigma_g$ and $1\sigma_u$ shells are in antiphase.

As an illustration we show in Fig. 1 the molecular frame photoelectron angular distributions (MFPADs) for electron energy 360 eV for three light polarizations. For light linearly polarized parallel to the molecular axis, the maximum of photoelectron intensity is directed along the molecular axis, and the Young interference is not visible since the dipole matrix element has a node in the plane perpendicular to the polarization direction, suppressing the first-order maxima. In contrast, when the light is linearly polarized perpendicular to the molecular axis, the photoelectrons are ejected mainly along the light polarization, and the angular distribution is essentially defined by the Young interference. As follows from Fig. 1(b), the interference maxima and minima appear

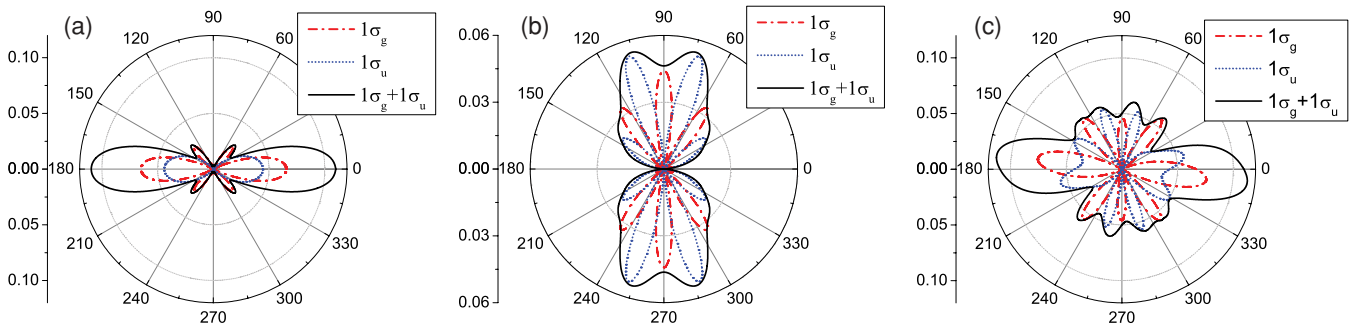

FIG. 1. (Color online) Molecular frame photoelectron angular distributions calculated for the photoelectron energy 360 eV and for absorption of light linearly polarized parallel (a) and perpendicular (b) to the molecular axis, and for left-handed circularly polarized light (c). The molecular axis is directed along the horizontal axis. The contributions of the $1\sigma_g$ and $1\sigma_u$ hole states are shown by dot-dashed (red) and dashed (blue) lines, respectively. Their sum is shown by the solid line.

exactly at the angles $\eta = \pm 17^\circ$ and $\eta = \pm 36^\circ$ in accord with our estimation, and oscillations for the $1\sigma_g$ and $1\sigma_u$ shells are in antiphase. And finally, for circularly polarized light shown in Fig. 1(c), the intensity can be qualitatively described as a sum of the contributions of the two linear polarizations considered above, slightly rotated in the direction of the light polarization. Qualitatively similar results have been obtained earlier for the photoelectrons from H_2 molecule [2]. To summarize, one can say that in photoionization the clearest Young interference pattern arises in the case of absorption of light linearly polarized perpendicular to the molecular axis. The corresponding patterns will be used in the following for comparison with the angular distributions of the Auger electrons. At the moment there are no experimental data for MFPADs for comparison with our calculations at this photon energy.

III. AUGER-ELECTRON ANGULAR DISTRIBUTIONS

The appearance of the Young interference pattern in the molecular frame Auger electron angular distributions (MFAADs) is less evident. The Auger electron is emitted from a valence shell where the electron density is not as strongly localized in the vicinity of each nucleus as it is in the $1\sigma_g$ and $1\sigma_u$ shells. Nevertheless, as our calculations show, the two-center character of the wave functions involved in the Auger decay is frequently sufficient to produce the Young interference patterns in the MFAADs, too. We attribute this to an overlap integral with the well centered innershell initial hole state in the Auger matrix element. This effectively confines the region from where the Auger electron is emitted tightly to the two nuclei.

Figure 2 shows the MFAADs for three Auger transitions compared to the MFPADs with the same electron energy 360 eV. The Young interference oscillations are the dominant features of these MFAADs in the broad range of angles from about 30° to 150°. As in the case of MFPADs, the positions of the main minima and maxima of the MFAADs fit well the estimated angles of $\eta = \pm 17^\circ$ and $\eta = \pm 36^\circ$ relative to the direction perpendicular to the molecular axis. All

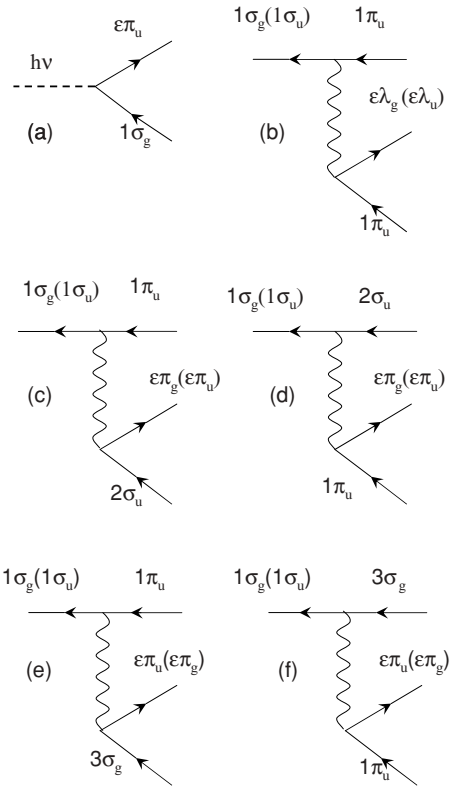

FIG. 3. Diagrams representing different photoionization and Auger-decay processes described in the text. Dashed line corresponds to a photon, wavy line denotes the Coulomb interaction, and solid lines correspond to a particle or a hole state.

these calculations have been performed at a fixed internuclear distance $R = 2.068$ a.u. corresponding to the ground state of the N_2 molecule.

To discuss in more detail these angular distributions, let us consider the lowest-order diagrams describing the photoionization and Auger-decay processes shown in Fig. 3 for the case of ionization of the $1\sigma_g$ ($1\sigma_u$) shell. The photoionization process is described by the diagram shown in Fig. 3(a). The

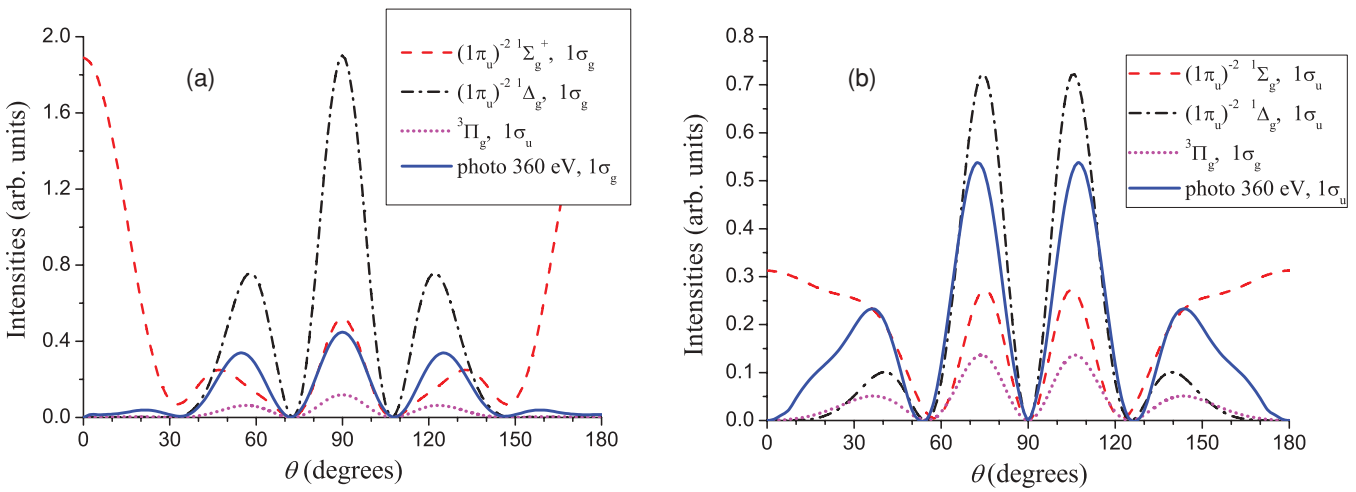

FIG. 2. (Color online) Comparison between the molecular frame photoelectron and Auger-electron angular distributions for equal electron energy 360 eV for the case of ionization of the $1\sigma_g$ shell (a) and $1\sigma_u$ shell (b) (and vice versa for the $^3\Pi_g$ state; see text for details).

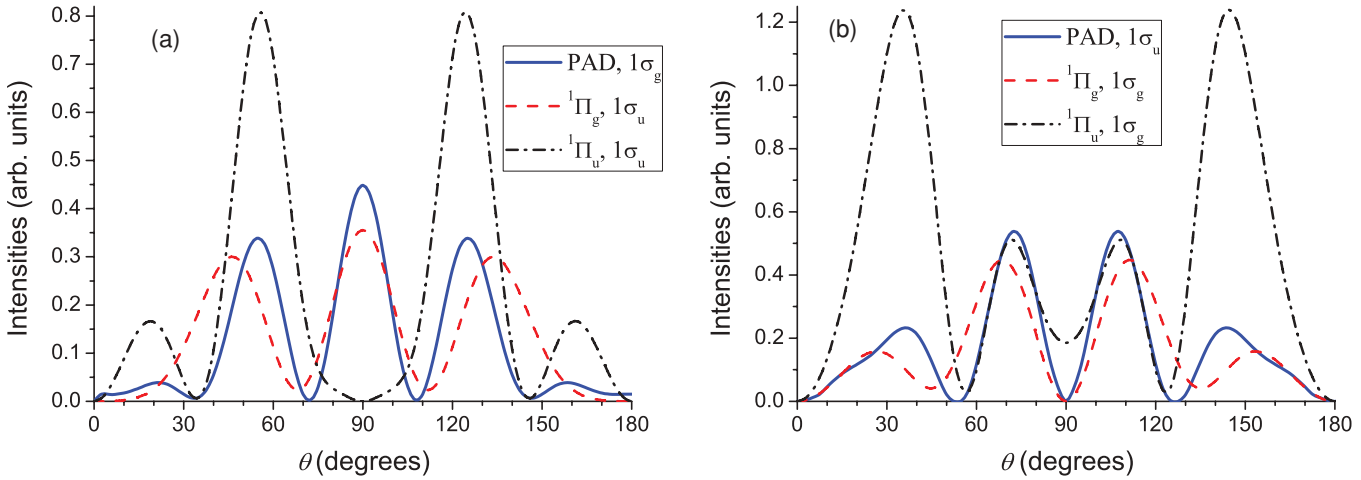

FIG. 4. (Color online) Examples of the molecular frame Auger-electron angular distributions deviating from the simple Young interference patterns exhibited by photoelectrons of equal energy ejected from the $1\sigma_g$ shell (a) and $1\sigma_u$ shell (b) (see text for details).

photoelectron wave ejected from the $1\sigma_g$ hole state for the case of light polarized perpendicular to the molecular axis ($\varepsilon\pi_u$ wave) when presented as an expansion in partial waves contains the sum of terms proportional to the spherical harmonics $Y_{11}, Y_{31}, Y_{51}, \ldots$. They all are proportional to $\sin\theta$ (θ is the polar angle in the molecular frame with the z axis directed along the molecular axis) and go to zero in the direction of the molecular axis. In the direction perpendicular to the molecular axis, that is, at $\theta = \pi/2$, they all have a maximum. The Auger decay of the $1\sigma_g$ hole leading to the $(1\pi_u)^{-2}\ {}^1\Sigma_g^+$ doubly charged ion state is described by the diagram shown in Fig. 3(b). From parity conservation, it follows that the Auger-electron wave function must correspond to the $\varepsilon\sigma_g$ wave [$\lambda_g = 0$ in Fig. 3(a)]. The partial wave expansion of this wave function includes the spherical harmonics $Y_{00}, Y_{20}, Y_{40}, \ldots$. They have maxima (except for Y_{00} which is constant at all angles) at the angle $\theta = \pi/2$, as well as at the angles $\theta = 0$ and π. The latter property explains the main difference between the $(1\pi_u)^{-2}\ {}^1\Sigma_g^+$ term and all others shown in Fig. 2, namely, that for the Σ term there is a maximum in the direction of the molecular axis where the MFAADs for the Δ and Π terms go to zero.

The Auger decay of the $1\sigma_g$ hole into the $(1\pi_u)^{-2}\ {}^1\Delta_g$ doubly charged ion state is described by the same diagram of Fig. 3(b) with $\lambda_g = 2$ producing the Auger electron in the $\varepsilon\delta_g$ state. Its expansion in partial waves contains the terms proportional to $Y_{22}, Y_{42}, Y_{62}, \ldots$. They all are proportional to $\sin^2\theta$, leading to zero along the molecular axis and to a maximum at $\theta = \pi/2$. And finally, the Auger decay of the $1\sigma_g$ hole into the $(2\sigma_u)^{-1}(1\pi_u)^{-1}\ {}^3\Pi_g$ final state is described by a difference of the diagrams shown in Figs. 3(c) and 3(d). In both cases the Auger electron is in the $\varepsilon\pi_g$ state, and its expansion in partial waves includes the spherical harmonics $Y_{21}, Y_{41}, Y_{61}, \ldots$. They all are proportional to the product $\sin\theta\cos\theta$, which gives zero intensity at the angle $\theta = \pi/2$, while other angular distributions for the $1\sigma_g$ hole state discussed above have a maximum at $\theta = \pi/2$. Therefore, for comparison with the angular distributions shown in Fig. 2(a), we must consider the Auger decay of the $1\sigma_u$ hole creating the Auger electron in the $\varepsilon\pi_u$ state. Then its partial wave expansion contains the spherical harmonics $Y_{11}, Y_{31}, Y_{51}, \ldots$, similarly to the photoelectron ejected from the $1\sigma_g$ shell, and the corresponding MFAAD behaves like the other angular distributions shown in Fig. 2(a), while the MFAAD from the $1\sigma_g$ hole leading to the $(2\sigma_u)^{-1}(1\pi_u)^{-1}\ {}^3\Pi_g$ final state behaves like the MFPAD from the $1\sigma_u$ shell and is shown in Fig. 2(b). An analogous treatment is applicable for explanation of the MFAADs from the decay of the $1\sigma_u$ hole state.

As was already mentioned, the MFAADs do not necessarily display the pure Young interference pattern as in the case of the MFPADs. We found that the MFAADs for the ${}^1\Pi_{g,u}$ final states do not follow as closely the Young interference patterns as those MFAADs shown in Figs. 2(a) and 2(b). These MFAADs are shown in Figs. 4(a) and 4(b). In the case of the $(2\sigma_u)^{-1}(1\pi_u)^{-1}\ {}^1\Pi_g$ state, the MFAAD is defined by the sum of the diagrams shown in Figs. 3(c) and 3(d), and has another period of oscillations as compared to the MFPAD also shown in Fig. 4. In the case of the $(3\sigma_g)^{-1}(1\pi_u)^{-1}\ {}^1\Pi_u$ final state, the MFAAD is defined by the sum of the diagrams shown in Figs. 3(e) and 3(f), and differ more substantially from the MFPAD. It is worthwhile to mention that the corresponding MFAADs for the triplet states ${}^3\Pi_{g,u}$ are defined by the difference of the diagrams shown in Figs. 3(c), 3(d) and 3(e), 3(f), and demonstrate a great similarity with the MFPADs, as was shown for the the $(2\sigma_u)^{-1}(1\pi_u)^{-1}\ {}^3\Pi_g$ final state in Figs. 2(a) and 2(b).

IV. KINETIC ENERGY RELEASE DEPENDENCE OF THE INTERFERENCE MAXIMA

Young-type interference in optics depends on the slit distance. Hence it is tempting to search for a dependence of the maxima in the photo- and Auger-electron angular dependence on internuclear distance of the molecule. Calculations for photoelectrons from H_2 have shown such a dependence recently [3,4]. For repulsive final states, the internuclear distance at the instant of the electronic transition is related to the kinetic energy release (KER). A classical approximation to this relationship of KER to R is given by the reflection approximation [34]. This has been used also to experimentally observe dependences of the Young-type interferences on the

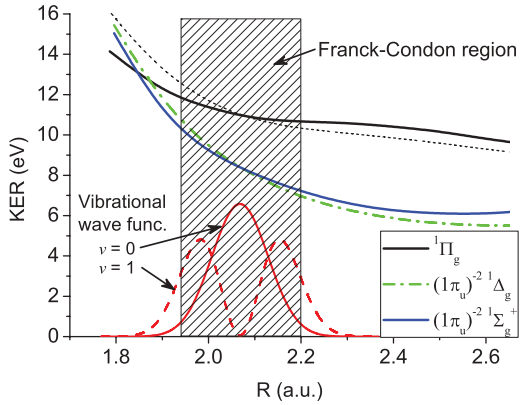

FIG. 5. (Color online) Potential energy curves from Refs. [30–33] for several final dicationic states mentioned in the figure. For estimation of the range of R accessible in the Auger-decay processes, the square moduli of the first two vibrational wave functions with $v = 0$ and 1 of the ground state of the N_2 molecule are also shown. For the $^1\Pi_g$ final state two curves are shown, one from Ref. [32] (bold solid curve) and the other from Ref. [33] (thin dashed curve).

KER [5,35]. For Auger electrons, however, no such study has been available so far to our knowledge.

From the known behavior of the molecular terms as a function of R [30–33] one can connect the KER of the atomic ions with the internuclear distance R. In Fig. 5 we show three molecular terms, the contributions of which can be traced from the experimental data. For estimation of the range of R accessible in the processes under investigation, the square moduli of the vibrational wave functions of the ground state of the N_2 molecule are also shown there. The analysis of the MFAAD at different KER performed in I shows that usually several transitions are contributing in a given narrow region of KER. Nevertheless, in some cases there are regions of angles where the predominant contribution is given by a single decay channel. In particular, as follows from Fig. 7(a) of I, in the Auger decay of the $1\sigma_g$ shell at a KER (E_K) in the region 10.2–11 eV, the predominant contribution at the angles 60°–75° and 105°–120° is given by the $(2\sigma_u)^{-1}(1\pi_u)^{-1}\ ^1\Pi_g$ final state.

Let us study the contribution of this final state in more detail. Figure 6 shows the theoretical MFAAD for this state calculated at several internuclear distances R. The positions of the main lobes are notably moving as a function of R. It is possible to analyze the experimental MFAADs as a function of KER in a much narrower KER region than was done in I. In Fig. 7 we show the modified Fig. 4(a) of I where a

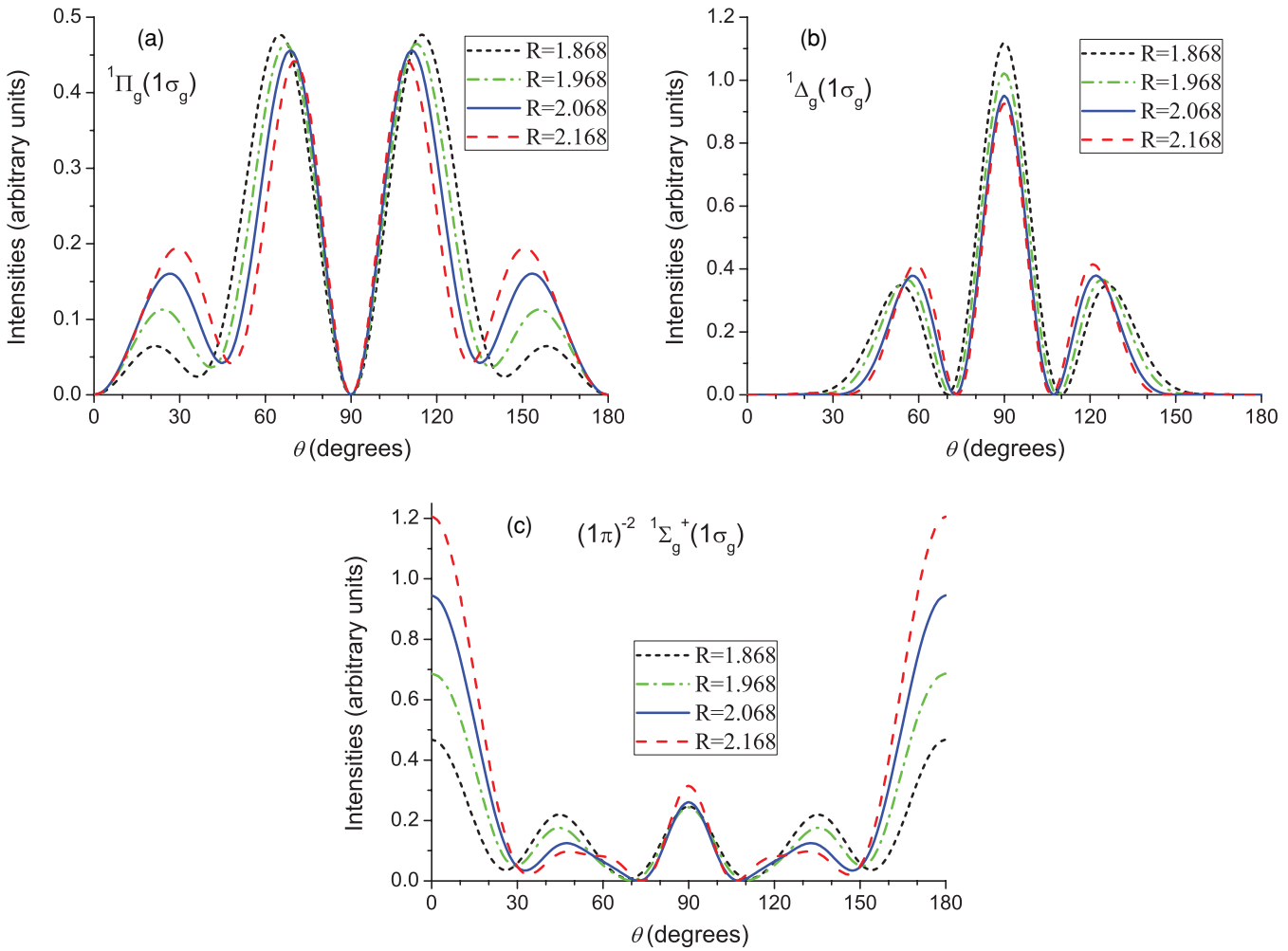

FIG. 6. (Color online) Theoretical molecular frame Auger-electron angular distributions for the decay of the $1\sigma_g$ hole into the $(2\sigma_u)^{-1}(1\pi_u)^{-1}\ ^1\Pi_g$ (a), $(1\pi_u)^{-2}\ ^1\Delta_g$ (b), and $(1\pi_u)^{-2}\ ^1\Sigma_g^+$ (c) final states calculated at several internuclear distances R mentioned in the figure.

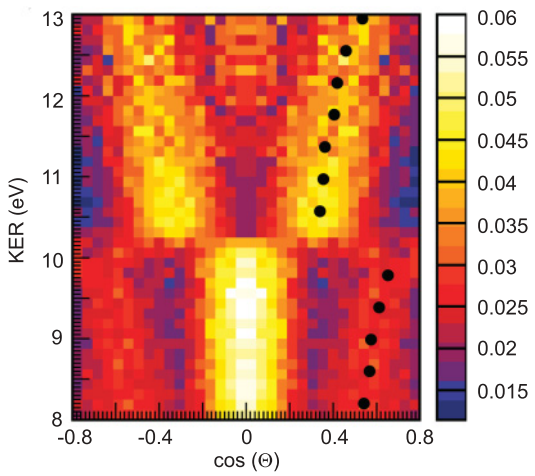

FIG. 7. (Color online) Experimental MFAAD as a function of KER. The total intensity at each KER value (each horizontal line) is normalized to unity. The black dots show the positions of the maxima obtained by fitting a Gaussian.

different normalization is used, namely, the total intensity at each KER value (each horizontal line) is normalized to unity. Owing to that, one can follow the positions of lobes up to the KER values as high as 13 eV. The fitted peak positions of lobes are shown in Fig. 7 by black points. In Fig. 8 we compare these positions with the corresponding theoretical values taken from Fig. 6. Up to $E_K = 12$ eV, there is a good agreement between theory and experiment, while at higher E_K the experimental points start to deviate from the theory. This is explained by a sharp decrease of the relative contribution of the $(2\sigma_u)^{-1}(1\pi_u)^{-1}\,{}^1\Pi_g$ final state to the total Auger-electron intensity as it is seen in Fig. 8 of I. As a result, the contribution of the $(1\pi_u)^{-2}\,{}^1\Delta_g$ final state is becoming comparable with that of the $(2\sigma_u)^{-1}(1\pi_u)^{-1}\,{}^1\Pi_g$ one, which is proved also by the appearance of the characteristic maximum at $E_K > 11.5$ eV at the angle $\theta = \pi/2$ ($\cos\theta = 0$) in Fig. 7. The positions of the theoretical first-order maxima of the $(1\pi_u)^{-2}\,{}^1\Delta_g$ final state are also shown in Fig. 8. The experimental points at $E_K > 12.5$ eV

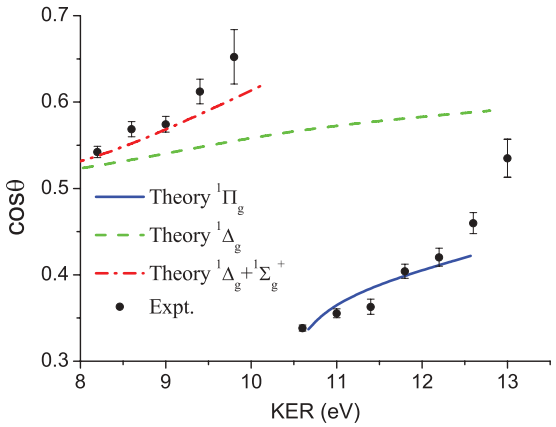

FIG. 8. (Color online) The experimental positions of lobes shown in Fig. 7 by black points, compared with the corresponding theoretical values shown in Fig. 6. The experimental points and error bars are obtained from a least sqare fit of of a gaussian on a flat background to the data.

evidently tend to the theoretical curve describing the positions of the lobe produced by the $(1\pi_u)^{-2}\,{}^1\Delta_g$ final state.

At $E_K > 12$ eV the $v = 0$ vibrational wave function is already too small to give a visible contribution to the Auger-electron intensity. Therefore most probably the contribution of the ${}^1\Delta_g$ term at these KERs is appearing due to the population of the $v = 1$ vibrationally excited state in the photoionization step. A high probability of its excitation was well established in a recent experimental and theoretical study [17]. The square modulus of the $v = 1$ vibrational wave function shown in Fig. 5 demonstrates that this explanation is feasible. At KER values in the region between 8 and 10 eV one can study the behavior of the lobes at $\cos\eta \approx \pm 0.6$. As follows from the study performed in I, the main contribution to it is given by the $(1\pi_u)^{-2}\,{}^1\Delta_g$ state, although the contribution of the $(1\pi_u)^{-2}\,{}^1\Sigma_g^+$ state cannot be neglected. The sum of these two contributions is shown in Fig. 8 together with the corresponding experimental points. There is a satisfactory agreement between the theory and experiment.

V. CONCLUSIONS

We have demonstrated that at electron energy 360 eV both photoelectron and Auger-electron angular distributions from the N_2 molecule can be reasonably well modeled by the Young interference of electron waves in a broad range of angles about the direction perpendicular to the molecular axis. At that energy the electron wavelength is comparable with the internuclear distance of the molecule, which makes the interference particularly strong. In our experiment the Auger-decay process was studied by detecting in coincidence the photoelectron, the Auger electron, and the two atomic singly charged ions, all of them being energy and angular resolved. This measurement made it possible to investigate the MFAAD in the molecule fixed frame as a function of the KER. Since different KER values correspond to different internuclear distances R at the moment of the Auger decay, it opens the possibility of experimental study of the Auger-decay process as a function of R. From the measured dependence of the positions of the Young interference maxima in the MFAADs on the KER value, one can disentangle the contribution of particular Auger-decay processes as a function of R. The measurements clearly demonstrated this dependence, in a good agreement with the predictions of our calculations. As a matter of fact, this method gives the possibility of an experimental check of the behavior of different molecular terms.

ACKNOWLEDGMENTS

We acknowledge outstanding support by the staff of the Advanced Lights Source, in particular by Hendrik Bluhm and Tolek Tyliszczak. The work was supported by the Deutsche Forschungsgemeinschaft and by the office of Basic Energy Sciences, Division of Chemical Sciences of the US DOE under Contracts No. DE-AC03-76SF00098 and No. DE-FG02-07ER46357. N.A.C. acknowledges the financial support of Deutsche Forschungsgemeinschaft. S.K.S. and N.A.C. acknowledge the hospitality of the Goethe University in Frankfurt am Main and the financial support of RFBR (Grant No. 09-03-00781-a).

[1] I. G. Kaplan and A. P. Markin, Dokl. Akad. Nauk SSSR **184**, 66 (1969) [Sov. Phys. Dokl. **14**, 36 (1969)].
[2] J. Fernandez, F. L. Yip, T. N. Rescigno, C. W. McCurdy, and F. Martin, Phys. Rev. A **79**, 043409 (2009).
[3] J. Fernandez, O. Fojon, and F. Martin, Phys. Rev. A **79**, 023420 (2009).
[4] J. Fernandez, O. Fojon, A. Palacios, and F. Martin, Phys. Rev. Lett. **98**, 043005 (2007).
[5] M. S. Schöffler *et al.*, Phys. Rev. A **78**, 013414 (2008).
[6] K. Kreidi *et al.*, Phys. Rev. Lett. **100**, 133005 (2008).
[7] K. Kreidi *et al.*, Eur. Phys. J. Spec. Top. **169**, 109 (2009).
[8] D. Akoury *et al.*, Science **318**, 949 (2007).
[9] D. A. Horner, S. Miyabe, T. N. Rescigno, C. W. McCurdy, F. Morales, and F. Martin, Phys. Rev. Lett. **101**, 183002 (2008).
[10] H. D. Cohen and U. Fano, Phys. Rev. **150**, 30 (1966).
[11] O. A. Fojon, J. Fernandez, A. Palacios, R. D. Rivarola, and F. Martin, J. Phys. B **37**, 3035 (2004).
[12] S. K. Semenov, N. A. Cherepkov, M. Matsumoto, T. Hatamoto, X.-J. Liu, G. Prümper, T. Tanaka, M. Hoshino, H. Tanaka, and F. Gel'mukhanov, J. Phys. B **39**, L261 (2006).
[13] X.-J. Liu, N. A. Cherepkov, S. K. Semenov, V. Kimberg, F. Gel'mukhanov, G. Prümper, T. Lischke, T. Tanaka, M. Hoshino, H. Tanaka, and K. Ueda, J. Phys. B **39**, 4801 (2006).
[14] N. Stolterfoht *et al.*, Phys. Rev. Lett. **87**, 023201 (2001).
[15] D. Misra, U. Kadhane, Y. P. Singh, L. C. Tribedi, P. D. Fainstein, and P. Richard, Phys. Rev. Lett. **92**, 153201 (2004).
[16] U. Hergenhahn, O. Kugeler, A. Rüdel, E. E. Rennie, and A. M. Bradshow, J. Phys. Chem. A **105**, 5704 (2001).
[17] S. K. Semenov *et al.*, J. Phys. B **39**, 375 (2006).
[18] A. V. Golovin, N. A. Cherepkov, and V. V. Kuznetsov, Z. Phys. D **24**, 371 (1992).
[19] E. Shigemasa, J. Adachi, M. Oura, and A. Yagishita, Phys. Rev. Lett. **74**, 359 (1995).
[20] F. Heiser, O. Gessner, J. Viefhaus, K. Wieliczek, R. Hentges, and U. Becker, Phys. Rev. Lett. **79**, 2435 (1997).
[21] R. Dörner, V. Mergel, O. Jagutzki, L. Spielberger, J. Ullrich, R. Moshammer, and H. Schmidt-Böcking, Phys. Rep. **330**, 95 (2000).
[22] S. Motoki, J. Adachi, Y. Hikosaka, K. Ito, M. Sano, K. Soejima, A. Yagishita, G. Raseev, and N. A. Cherepkov, J. Phys. B **33**, 4193 (2000).
[23] Th. Weber *et al.*, J. Phys. B **34**, 3669 (2001).
[24] M. Lebech, J. C. Houver, A. Lafosse, D. Dowek, C. Alcaraz, L. Nahon, and R. R. Lucchese, J. Chem. Phys. **118**, 9653 (2003)
[25] M. S. Schöffler *et al.*, Science **320**, 920 (2008).
[26] N. A. Cherepkov *et al.*, Phys. Rev. A **80**, 051404(R) (2009).
[27] S. K. Semenov *et al.*, Phys. Rev. A **81**, 043426 (2010).
[28] J. Ullrich, R. Moshammer, A. Dorn, R. Dörner, L. Ph. H. Schmidt, and H. Schmidt-Böcking, Rep. Prog. Phys. **66**, 1463 (2003).
[29] T. Jahnke, Th. Weber, T. Osipov, A. L. Landers, O. Jagutzki, L. Ph. H. Schmidt, C. L. Cocke, M. H. Prior, H. Schmidt-Böcking, and R. Dörner, J. Electron Spectrosc. Relat. Phenom. **141**, 229 (2004).
[30] M. Lundqvist, D. Edvardsson, P. Baltzer, and B. Wannberg, J. Phys. B **29**, 1489 (1996).
[31] E. W. Thulstrup and A. Andersen, J. Phys. B **8**, 965 (1975).
[32] P. R. Taylor, Mol. Phys. **49**, 1297 (1983).
[33] R. W. Wetmore and R. K. Boyd, J. Phys. Chem. **90**, 5540 (1986).
[34] E. A. Gislason, J. Chem. Phys. **58**, 3702 (1973).
[35] L. Ph. H. Schmidt, S. Schössler, F. Afaneh, M. Schöffler, K. E. Stiebing, H. Schmidt-Böcking, and R. Dörner, Phys. Rev. Lett. **101**, 173202 (2008),